https://doi.org/10.5194/egusphere-2026-3247
Preprint. Discussion started: 13 July 2026

A Model for Antarctic Ice Shelf Hydrology and Stability (MONARCHS v1.0)

Sammie Buzzard[1,2], Jonathan Elsey[3,4], and Alexander Robel[2]

[1]Centre for Polar Observation and Modelling, Department of Geography and Natural Sciences, Northumbria University, UK
[2]School of Earth and Atmospheric Sciences, Georgia Institute of Technology, USA
[3]Research Software Engineering, Newcastle University, UK
[4]School of Earth and Environmental Sciences, Cardiff University, UK

Correspondence: Sammie Buzzard (sammie.buzzard@northumbria.ac.uk)

Abstract. Antarctica's floating ice shelves experience considerable surface melting, leading to the formation of supraglacial melt lakes. The presence of surface meltwater and the formation of these lakes leaves ice shelves vulnerable to meltwater-induced damage. This can lead to the loss of the buttressing effect provided by ice shelves on the grounded ice sheet, thus increasing Antarctica's potential sea level contribution. Understanding the surface hydrology of ice shelves in the present and the future is thus an essential first step to reliably project future vulnerability of Antarctic ice shelves to meltwater-driven hydrofracture and possible collapse events. Therefore, we have developed the first comprehensive 3-D Model for Antarctic Ice Shelf Hydrology and Stability, called MONARCHS.

MONARCHS calculates the surface energy balance of the ice shelf, heat transfer through the ice shelf and the volume of any subsequent meltwater that is produced when the surface energy balance is positive. The model simulates both vertical and lateral movement of this meltwater through the firn, calculating refreezing and saturation of firn air space as well the related changes in temperature and density. When firn is saturated and surface melt lakes can form, the model simulates the full lake lifecycle, including lake depth increases and full refreezing.

We present a case study focused on the George VI Ice Shelf on the Antarctic Peninsula where significant melt lake formation has been observed in recent years. The model shows reasonable agreement in lake extent and depth with observations. Furthermore, we demonstrate that the speed of lateral meltwater percolation through firn, a key uncertainty in firn modelling, has significant consequences for lake extent and depth, suggesting future research should focus on reducing this uncertainty. This community-driven, open-access model has been developed with input from observations, and will allows us to provide new insights into the surface meltwater distribution on Antarctica's ice shelves.

1 Introduction

Floating ice shelves surround 75% of the margin of the Antarctic Ice Sheet (Rignot et al., 2013). They modulate the flow of ice towards the ocean by restraining, or buttressing, the grounded ice sheet and are sensitive to changes in the atmosphere and ocean (Holland et al., 2015). The loss of ice shelves removes their buttressing effect on the grounded ice sheet which has been observed to cause acceleration of glacier flow, and corresponding sea level rise (Wuite et al., 2015). Uncertainty in the future

https://doi.org/10.5194/egusphere-2026-3247
Preprint. Discussion started: 13 July 2026

stability of ice shelves and the impact of this potential change in buttressing leads to large uncertainties in Antarctica's future sea level contribution (Fricker et al., 2025).

Melting on the surface of Antarctic ice shelves is much more extensive than previously thought (Bell et al., 2018). The formation of surface meltwater lakes has been linked with the disintegration of many ice shelves in the Antarctic Peninsula over the last several decades. The most notable ice shelf collapse occurred in 2002, when many thousands of meltwater lakes were observed on the surface of the Larsen B Ice Shelf before its collapse over a period of just a few weeks (Scambos et al., 2004). Several mechanisms have been proposed to explain the role of meltwater in sudden ice shelf collapse, including fracture networks caused by lake-induced flexural stresses (Banwell et al., 2013; Banwell and MacAyeal, 2015) and meltwater-driven propagation of crevasses through the ice shelf (Scambos et al., 2000).

Observational evidence indicates that even on ice shelves not experiencing surface melting, long distance water flow over the ice surface can import meltwater, lowering local albedo, and potentially causing an acceleration of ice loss in regions previously thought to be completely dry (Kingslake et al., 2017). Conversely, it has also been suggested that surface rivers may stabilize ice shelves by draining meltwater off the ice shelf (Bell et al., 2017). Surface melting on grounded ice also has the potential to influence ice sheet and thus ice shelf flow, for example in the Antarctic Peninsula (Boxall et al., 2022; Tuckett et al., 2019; Hanna et al., 2024).

Despite the importance of surface meltwater production, transport and ponding to ice shelf stability, understanding of these processes is still lacking. The way in which ice shelf surface melt is simulated varies strongly between models, leading to large variations in projections of the Antarctic contribution to sea level (DeConto and Pollard, 2016; Edwards et al., 2019). To date these processes have not been included (in a parameterized fashion or otherwise) in either ice sheet or climate models. Furthermore, climate models (CMIP5) have known biases in near-surface climate resulting from poor representation of ice sheet surface processes (Trusel et al., 2015), which in turn leads to biases in surface melt parameterizations.

Without including lateral transport of meltwater across ice shelves, models may overestimate their sensitivity to meltwater in some places (where water is removed by lateral transport), and underestimate their sensitivity in other places (where water is added by lateral transport). The accurate representation of surface hydrology and heat fluxes is essential in predicting the future stability of Antarctica's ice shelves, as has been argued in study after study (e.g., Hock (2005); Bell et al. (2017); Bell et al. (2018)), yet no current model of surface hydrology tackles these processes comprehensively.

The current most comprehensive surface lake development model for Antarctica, that of Buzzard et al. (2018a), simulates the surface energy balance and vertical heat and meltwater fluxes through the top of the ice shelf. An approximate catchment area for each modelled lake is calculated, but this was shown to lead to a high level of variability in the lake depths calculated (Buzzard et al., 2018a). Alternatively, simple diagnostic parameterizations of spatially-averaged supraglacial lake size metrics have been developed using models of water transport on ice-sheet-like rough surfaces (Grau et al., 2025). However, such parameterizations do not account for the production or refreezing of meltwater, nor do they incorporate how water percolates through firn, which has been identified as a bias in comparisons of these parameterizations to observations. Models developed for the Greenland Ice Sheet that do account for transport of meltwater across ice shelf or ice sheet surfaces (e.g. Leeson et al. (2012), Banwell et al. (2012), Gantayat et al. (2023), Clerx et al. (2024)) do not account for all of the full surface energy

https://doi.org/10.5194/egusphere-2026-3247
Preprint. Discussion started: 13 July 2026

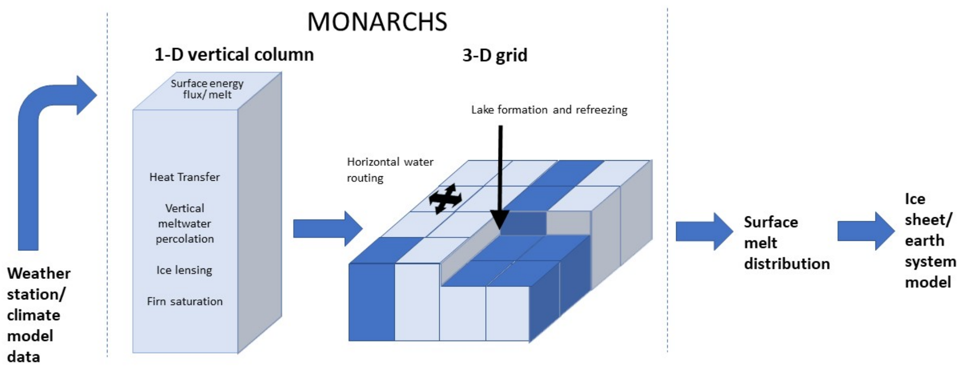

Figure 1. Schematic showing processes and information flow in MONARCHS.

balance, the complete lake lifecycle over multiple years (and the associated evolution in the ice shelf), or the retention of meltwater within firn.

The Antarctic research community has collectively indicated that key priorities for future research include: determining controls on the extent, variability, and magnitude of Antarctic surface melt, lakes and rivers; and the identification of ice shelves that are likely to accumulate meltwater in the future (Kingslake et al., 2019; The Firn Symposium Team, 2024). To address these priorities, we have developed a comprehensive model of Antarctic surface meltwater: MONARCHS (Model Of aNtARctic iCe shelf Hydrology and Stability). MONARCHS incorporates a surface energy balance calculation, meltwater production, the vertical and horizontal movement of meltwater, potential refreezing of meltwater and meltwater lake formation, expansion and refreezing. This enables the model to simulate meltwater lake evolution and distribution for any ice shelf in Antarctica.

This manuscript is organized as follows: in Section 2 we describe the model structure and constitutive equations; in Section 3 we outline model test cases; we present a case study in Section 4; we carry out model validation in Section 5 and discuss these results and their relationship to past research on supraglacial hydrology in Section 6.

2 Model Overview

The 1-D vertical column model of (Buzzard et al., 2018b), described in Section 2.1), calculates the surface energy balance of the ice shelf, the volume of any meltwater produced and the change in heat and density as water percolates down through the column. MONARCHS, shown in Figure 1, expands this column model to a 3-D numerical model of meltwater distribution within and on the surface of an ice shelf, allowing meltwater to move between columns.

https://doi.org/10.5194/egusphere-2026-3247
Preprint. Discussion started: 13 July 2026

Figure 2 shows the top-level structure of MONARCHS, including configuration steps, input/output and the model physics. When simulating processes occurring within a vertical column, each column is initially assumed to behave independently. Only after meltwater production and vertical water percolation rates have been calculated does the model consider the lateral movement of water between the columns at both the surface and subsurface, up to the pore closure depth, which here is defined as any vertical grid cell with a density of greater than 830 kg m^{-3}.

In order to account for the differences in spatial and temporal scale between the processes occurring in the vertical column model (∼cm, the scale of individual ice lenses), and processes occurring in the lateral transport model (∼100 m, the scale of lakes or larger), we implement asynchronous operator splitting to couple the vertical column model elements to the horizontal transport equations. The vertical column model has a short time step (∼hours) which is integrated multiple times between each lateral timestep (∼days), but the time steps and coupling frequency can be altered to suit the area and resolution of a given simulation.

Due to the large differences in scale between vertical and horizontal grid cells, only water is transported between vertical columns during the horizontal water routing routine, horizontal heat diffusion is assumed to be negligible. Such an assumption is reasonable since there are not strong differences in vertical and horizontal heat diffusivity and vertical gradient of temperature within snow, firn and ice are typically much larger than horizontal gradients, thus meaning that horizontal heat fluxes across 1D columns is negligible compared to vertical heat fluxes within columns. Enthalpy transport thus only occurs between columns as a result of water movement.

2.1 1-D firn, ice and lake model

The 1-D firn and ice column model of Buzzard et al. (2018a) forms the core of MONARCHS, and has been refactored into the Python programming language for efficiency, usability and accessibility. The column model still retains all the key physics of the Buzzard et al. (2018a) model, as demonstrated in Figure 3. Key parameters and typical values used in the results presented here are found in Appendix A.

During each timestep MONARCHS is run, the surface energy balance for each grid cell is calculated, and the processes shown in Figure 3 are incorporated where relevant, depending on whether the grid cell contains a lake or not. In the basic model state (no lake present) the surface energy balance is used to calculate the ice surface temperature ($T(z=0,t)$) according an implicit nonlinear equation:

$$\varepsilon F_{LW} + (1-\alpha)F_{SW} - \varepsilon\sigma T^4 + F_{Sens} + F_{Lat} = \begin{cases} k\frac{\partial T}{\partial z} + \phi\rho_{ice}\mathcal{L}\frac{dH}{dt}, & T = T_{frz}, \\ k\frac{\partial T}{\partial z}, & T < T_{frz}, \end{cases} \tag{1}$$

where T is temperature (K) (with T_{frz} being 273 K), ρ is density (kg m^{-3}), t is time (s), z is height (m), ε is the surface emissivity, α the surface albedo, F_{LW} and F_{SW} are the incoming longwave and shortwave energy (W m^{-2}), σ is the Stefan-Boltzmann constant (5.67×10^{-8} W m^{-2} K^{-4}) and F_{Sens} and F_{Lat} are the sensible and latent heat fluxes (W m^{-2}). On the right hand side, ϕ is the solid fraction of the firn which can take a value between 0 and 1, $\mathcal{L}$ is the latent heat of fusion as phase

https://doi.org/10.5194/egusphere-2026-3247
Preprint. Discussion started: 13 July 2026

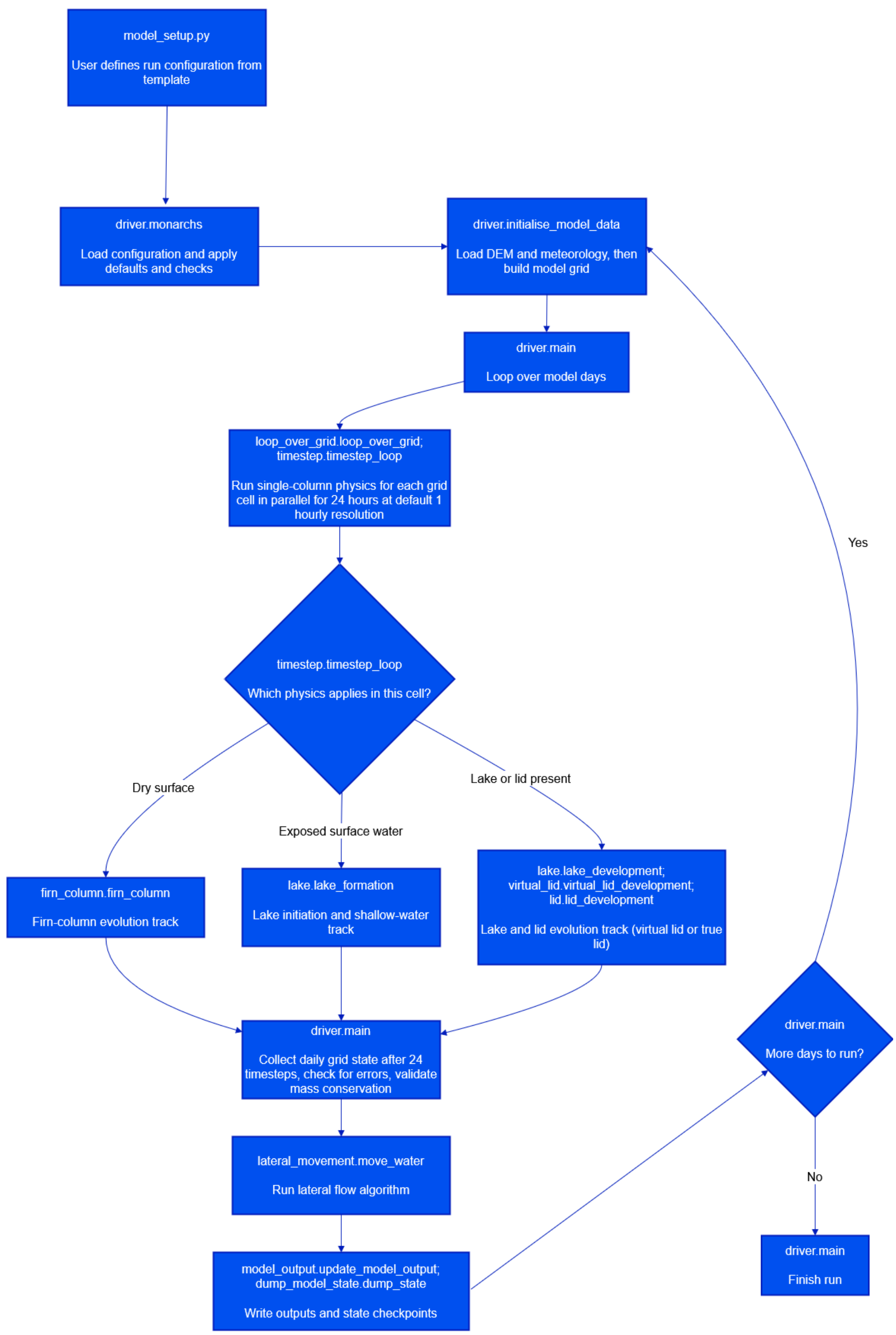

Figure 2. Flowchart showing the high-level workflow of MONARCHS, including configuration, data input, physics, output and validation steps.

https://doi.org/10.5194/egusphere-2026-3247
Preprint. Discussion started: 13 July 2026

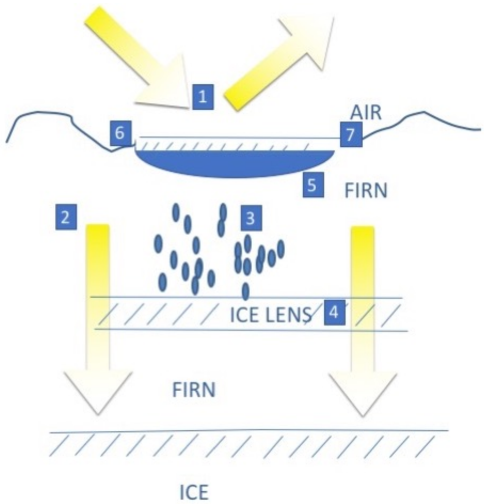

Figure 3. The key physical processes incorporated in the 1-D column model in MONARCHS: (1) The surface energy balance is calculated from input flux data; (2) Heat transfer through the firn; (3) Meltwater percolation into the firn and any refreezing (with subsequent density and temperature changes); (4) Formation of impermeable ice lenses from refrozen meltwater; (5) Formation of surface lakes, and their development through basal melting; (6) Refreezing of surface lakes; (7) Variations in surface albedo due to melting and lake formation are accounted for.

change occurs due to surface melting (J kg^{-1}) and k is thermal conductivity (W m^{-1} K^{-1}), calculated as a combination of the thermal conductivities of ice and air in a proportion determined by the value of ϕ.

Heat transfer through the firn is calculated following the heat equation:

$$\rho c_p \frac{\partial T}{\partial t} = \frac{\partial}{\partial z}(k \frac{\partial T}{\partial z}). \quad (2)$$

Here c_p is the specific heat capacity (J kg^{-1}K^{-1}), which, like k is calculated as a combination of the specific heat capacities of air and ice depending on the value of the solid fraction, ϕ. We assume that there is no heat transport through the bottom boundary of the model (i.e., $\frac{\partial T}{\partial z} = 0$). This assumption could be modified in the future if MONARCHS is coupled to a thermomechanical ice sheet model, but for standalone MONARCHS simulation it is a good approximation to assume no heat flux at depth.

Once melting occurs the meltwater will percolate vertically until it either reaches a vertical grid cell with a temperature below 273 K, where it will refreeze, or a grid cell with a density equal to or greater than the pore closure density, where it will remain as liquid, saturating the firn from that point upwards. Water remains at the melting point as it percolates, as we assume that heat advection via vertical percolation is negligible and that firn temperature changes are dominated by the latent heat release during phase change.

When the firn is fully saturated between the pore closure depth and the surface, a lake forms. Heating of the lake will lead to melting of the firn below. The surface energy balance at the lake surface is calculated as follows:

$$F_{LW} + (1-\alpha)F_{SW} - \epsilon\sigma T^4 - F_{Sens} - F_{Lat} + F_c(T_{sfc}) = 0. \quad (3)$$

https://doi.org/10.5194/egusphere-2026-3247
Preprint. Discussion started: 13 July 2026

F_c is the energy flux out of the lake, calculated using the four-thirds law for turbulent convection. Fluxes in and out of the lake are calculated following

$$F_c(T^*) = sgn(\bar{T} - T^*)(\rho c)_l J |\bar{T} - T^*|^{4/3}. \tag{4}$$

Here T^* is the boundary temperature (K), $\bar{T}$ is the average temperature in the lake (K), $(\rho c)_l$ is the volumetric specific heat capacity of water (J K^{-1} m^3) and J is the turbulent heat flux factor, 1.907 x 10 $^{-5}$ms^{-1}K$^{-1/3}$.

The movement of the lake-firn boundary is treated as a Stefan problem:

$$\phi \rho \mathcal{L} \frac{\partial h_l}{\partial t} = k \frac{\partial T}{\partial z} + F_c(T_l). \tag{5}$$

Here h_l is the location of the boundary between the lake and the firn, T_l is the temperature at that boundary and $\mathcal{L}$ is the latent heat of fusion due to phase change (J kg^{-1}).

If the lake temperature drops sufficiently that it starts to refreeze on its surface then a frozen ice lid will form. The lid-lake boundary development is also treated as a Stefan problem similarly to equation 6,

$$\phi \rho \mathcal{L} \frac{\partial h_u}{\partial t} = k \frac{\partial T}{\partial z} + F_c(T_u), \tag{6}$$

where h_u is the location of the boundary between the lake and the lid and T_u is the temperature at that boundary. For both the lake and lid cases, the temperature profile of the firn continues to be calculated as described above but with the temperature at the surface of the firn held at 273.15 K as this is a phase change boundary.

While the 1-D model solves the equations described above and in Buzzard et al. (2018b), we have made some updates to improve the model physics and allow for a wider range of applicability. In the original 1-D model code (Buzzard, 2017) melting and freezing at both the firn-lake and lake-lid boundaries were calculated using a purely conductive approach across the boundaries. In MONARCHS, we also model the turbulent fluxes at the boundary, resulting in a more accurate calculation of the net flux at the phase change boundaries and thus more accurate melting and freezing rates.

MONARCHS also uses a more sophisticated method to calculate the flux of shortwave radiation within the lake and lid. Previously, it was assumed that all shortwave radiation was absorbed by the surface, the energy then propagating into the system via the turbulent mixing scheme. In MONARCHS, when we have a lake, we split shortwave radiation into two bands - one band assumed to be absorbed entirely by the firn/ice/water surface (representing near-infrared, shortwave infrared and ultraviolet radiation). The remaining energy penetrates into the lake or lid, and is attenuated (distributing the energy throughout). Any energy remaining after this process will be either reflected back at the phase change boundary and absorbed into the lake, or absorbed, meaning its energy contributes directly to the energy balance used in the melting/freezing calculation. This split is assumed to be 50-50, calculated from spectral data in Pope and Fry (1997) and Kou et al. (1993), and as suggested in Leppäranta (2015). The liquid water attenuation coefficient is set to 0.36, taken from Table 1 of Pope et al. (2016), and the ice attenuation coefficient to 1.5, taken from Section 3 of Cooper et al. (2021). All of these parameters are defined in a module (`monarchs.physics.constants`), and can be changed by the user.

Additionally, we are now able to account for the presence of firn aquifers. Previously the 1-D model was able to simulate the full supraglacial lake life cycle, from formation to refreezing. However, should the lake not completely refreeze between melt

https://doi.org/10.5194/egusphere-2026-3247
Preprint. Discussion started: 13 July 2026

seasons, the model was unable to account for the presence of a subsurface lake or firn aquifer persisting through to the next melt season. At the time of publication of Buzzard et al. (2018b) there was no evidence that lakes would persist between melt seasons on the Larsen C Ice Shelf, the study site. However, van Wessem et al. (2021) suggested that perennial firn aquifers could be present on the Antarctic Peninsula and Dunmire et al. (2020) found evidence of buried Antarctic supraglacial lakes, after Buzzard et al. (2018a) had suggested that changes in the climate of the Antarctic Peninsula in the range of the those predicted for future decades could lead to conditions where supraglacial lakes do not completely freeze through between melt seasons. Furthermore, föhn winds have been observed to cause wintertime melt on the Larsen C Ice Shelf (Kuipers Munneke et al., 2018). Therefore, we now allow lakes in MONARCHS remain partially unfrozen, with new lakes allowed to form above partially frozen lakes, with the partially frozen lake incorporated into the firn as a vertical model layer with a liquid fraction of 1. While it is beyond the scope of this current work to fully account for subsurface lakes and their associated physics, this simplified method allows us to run MONARCHS into the future and understand how and where these features may occur.

Finally, the original 1-D model used a "melt multiplier" variable to account for the input of meltwater from lateral movement of water through the firn. We now account for the lateral transport of water through firn, as described in Section 2.2.

2.2 Horizontal Water Routing

Horizontal water routing occurs after a defined number of time steps of the vertical column model described in Section 2.1. Each column in MONARCHS is assigned a potential surface height from which water will move, which will either be the lake surface (if one is present), or the highest of either the pore closure depth, an impermeable ice lens or the top of the saturated firn in the presence of wet snow or firn.

The modelling approach for lateral water transport is adapted from prior cellular automata approaches for landscape hydrology (e.g. Chase (1992); Coulthard et al. (2002)). Water moves from a cell to the adjacent cell with the lowest height, should a neighbour exist with a height lower than the cell in question. If two or more neighbouring cells should have the same lower height water will be distributed to them equally. An illustration of horizontal water routing is shown in Figure 4. The selection of locations to move to is carried out following a D8 algorithm, meaning that water can move to any of the eight neighboring cells of the cell in question.

Current firn models struggle to capture lateral flow processes (The Firn Symposium Team, 2024), so here we calculate lateral flow using bulk properties of the firn. If water is moving horizontally below the surface through firn then the speed of percolation is calculated according to Darcy's Law of fluid flow through a porous medium (Colbeck, 1978) in the following formulation,

$$u = \frac{\Pi}{\eta} \rho_{firn} g \Delta H, \tag{7}$$

where u is the flow speed (m s^{-1}), Π is the hydraulic permeability, (-2.53x10^{-10}m^2), η is the viscosity (1.787x10^{-3}Pa s^{-1}), the density ρ_{firn} is the density of the firn layer the water is moving through and ΔH is the vertical gradient the water is travelling down.

https://doi.org/10.5194/egusphere-2026-3247
Preprint. Discussion started: 13 July 2026

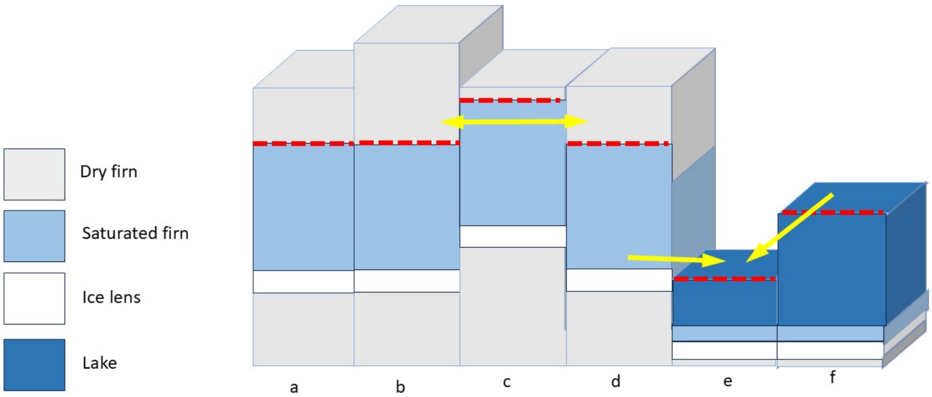

Figure 4. The process of lateral flow shown on a 6 x 1 example grid. Here the red dashed lines show the height used for each column in determining the direction of water routing and yellow arrows show water movement. Water from column c will move through the firn to both columns b and d as both a and c are at equal heights. No water moves between a and b as they are at the same height. Water in the saturated firn in column d will move to the lake in column e and water from the lake in column f will move to the lower lake in column e.

The horizontal grid cell size of the model (usually of the order of 10^2 to 10^3 m) will generally far exceed the vertical (10^{-2} to 10^{-1} m). Thus, we expect that only a small proportion of the meltwater present in a grid cell will leave the cell during a single horizontal timestep. The proportion of available meltwater that will be transferred to a neighbouring cell is determined by the total amount that could possibly move within the lateral timestep according to Darcy's Law, equation 7, if water is assumed to flow for the entire lateral timestep. Thus we have:

$$w_{move} = u * \Delta t_{lat}/l, \tag{8}$$

where w_{move} is the fraction of total water available to be transported that moves, Δt_{lat} is the lateral timestep (seconds) and l is the distance between the centrepoints of the lateral grid cells the water is moving from and to (meters). In the case of lake water movement it is assumed that all water in a cell that can move will move, since the hydraulic permeability of water along a free surface is effectively infinite.

For the case studies presented in Section 4, it is assumed water does not leave the model domain through the lateral boundaries. We consider this as a good assumption, since for the George VI Ice Shelf we examine a domain where the ice shelf surface meets land at a higher elevation. However, MONARCHS is not restricted to this behaviour and can be changed to allow either a proportion of water to leave the model domain at the boundaries (which can be specified based on the surrounding topography) or to allow all water to leave at a boundary if the boundary is the calving front of the ice shelf.

2.3 Computational Considerations

MONARCHS has been fully developed in Python 3 (Van Rossum and Drake, 2009) and all libraries used in MONARCHS are non-proprietary. Python was chosen due to its ease of use (for both development of the source code and for debugging) relative to languages such as C and Fortran, its extensive library support, and the fact that it is open source (unlike MATLAB, used in Buzzard et al. (2018b)). However, compared to C and Fortran, Python is comparatively slow. To account for this, MONARCHS has optional support for just-in-time (JIT) compilation via Numba (Lam et al., 2015). This feature can be enabled via the use_numba flag. Enabling this feature may hinder troubleshooting of code, but significantly improves performance. This performance increase scales with the number of lateral grid cells and time steps used when running the model. The model has been tested on Mac, Linux and Windows operating systems; however for the optimisations provided by Numba to work, a working Fortran compiler must be installed on the system (since MONARCHS uses a Python wrapper around the Fortran MINPACK library when running with Numba enabled). Where this is not available, the model will fall back to using an implementation using scipy.optimize.fsolve, which also wraps MINPACK, but is not compatible with Numba. While Numba adds approximately 1-2 minutes of front-loaded overhead to a model run, since the code is just-in-time compiled before running, the performance benefits significantly outweigh this overhead when running over large domains or for long periods of time.

MONARCHS and the MATLAB model of Buzzard et al. (2018b) are not directly comparable due to the significantly different code structure of MONARCHS including the use of different numerical solvers for the heat equation. Nevertheless, for simple test cases, similar results are obtained, but with MONARCHS having significantly better computational performance compared to the MATLAB model. When running a 140-day 1-D column case MONARCHS with Numba JIT compilation performs approximately 100 times faster than the MATLAB model (excluding Numba compile time, see figure 5). Using the slower scipy solver produces a six-fold speed up compared to Buzzard et al. (2018b).

The computational expense associated with running MONARCHS is primarily associated with the vertical column model elements, which within a model timestep are calculated independently from each other; information is only passed between the columns in the lateral movement step. Thus, this problem is embarrassingly parallelizable. MONARCHS has native support for shared-memory parallelism via Numba's `prange` function, or if running without Numba optimisations, via Python's inbuilt `multiprocessing` library. This approach allows us to balance performance considerations with the desire for the code to be accessible and editable by researchers, particularly those who do not have significant parallel programming experience.

To prevent issues with dependencies, and make it easier to use on HPC systems, a Docker image is available, which contains a working version of the model, which can be run on HPC using `apptainer`. Alternatively, MONARCHS is fully installable alongside all of its dependencies using `pip`.

2.3.1 Parallel performance

In order to test the ability of MONARCHS to scale with increasing computational resources, a test case with three firn depressions (see Section 3.2) with 2500 grid points was run with a varying number of CPUs to test strong scaling on a 64-core

https://doi.org/10.5194/egusphere-2026-3247
Preprint. Discussion started: 13 July 2026

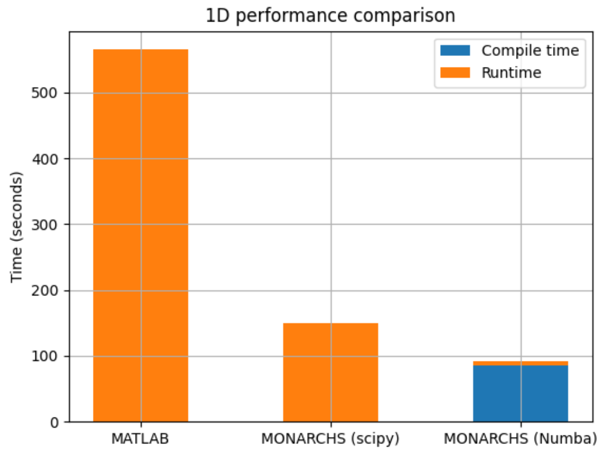

Figure 5. 1D performance of the MATLAB model of Buzzard et al. (2018b) vs. MONARCHS in the two available configurations, for a 1D test case with 140 timesteps. In the Numba case, the first timestep takes around 85 seconds to run since it needs to compile the MONARCHS code, but subsequent timesteps take around 0.02 seconds to run.

Linux server over 105 modelled days. The meteorological conditions in this experiment were chosen to force lake and lid formation, to ensure that the full range of computational regimes was represented in the experiment. Figure 6 shows the time taken to complete this test simulation. In these experiments, lateral movement contributes approximately 0.1s per timestep, serial processing (e.g. I/O) approximately 0.2s per timestep, and single-column physics the remainder, varying from around 10-0.5 seconds as the number of CPUs increases.

Figure 7 shows a similar experiment, but with a varying number of grid points, such that the overall work per processor is balanced (64 columns per processor), in order to test weak scaling.

The falloff in the scaling is due to two factors. Firstly, there are several components of the model that cannot be easily parallelised, such as writing dumps and output files to netCDF format, logging and diagnostics. Thus, while the single-column performance scales quite well, there are serial components that do not scale with increased computing resource. Secondly, there is some inefficiency in the parallel processing, likely due to a combination of threading overhead and load imbalance, as the work-per-column will be different depending on the model state (e.g. whether lids or lakes are present in a particular column). Nevertheless, for the range of CPU counts that we present here, MONARCHS scales well, enabling us to run large simulations in reasonable timeframes. As the model is in continuous development, future work will continue to improve performance and parallel scaling, enabling us to consider larger problems (both in terms of resolution and domain size).

https://doi.org/10.5194/egusphere-2026-3247
Preprint. Discussion started: 13 July 2026

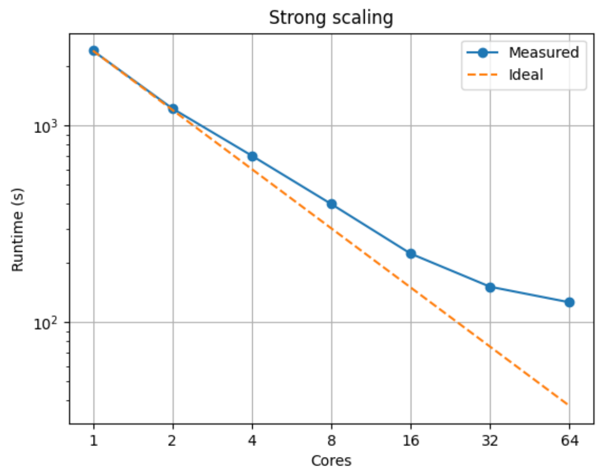

Figure 6. Strong scaling (fixed problem size, varying computational resource) for MONARCHS.

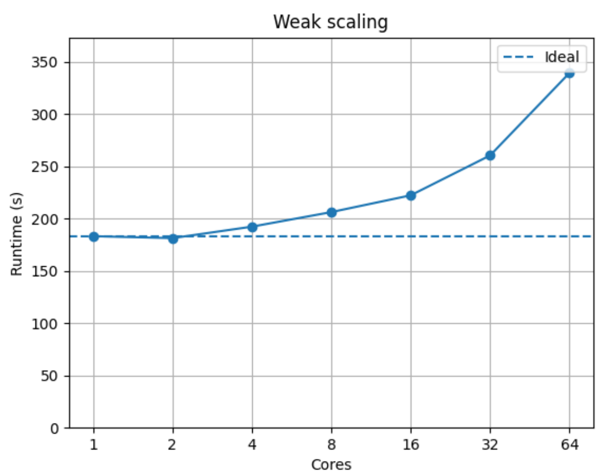

Figure 7. As in Figure 6, but for a weak scaling experiment (where problem size scales with compute resource).

https://doi.org/10.5194/egusphere-2026-3247
Preprint. Discussion started: 13 July 2026

Number of vertical points	Initial Δz (cm)	Firn depth (m)	Lake depth (m)	Lid depth (m)	Total melt (m)
50	70	25.659273	1.766475	1.604638	6.8642
100	35	25.583110	1.948383	1.598805	6.9657
150	23.33	25.564315	1.996556	1.597362	6.9896
200	17.50	25.555829	2.016880	1.596672	6.9993
300	11.66	25.551274	2.029116	1.596570	7.0035
500	7.00	25.542611	2.048835	1.595886	7.0123
750	4.66	25.547116	2.044527	1.595928	7.0067
1000	3.50	25.523331	2.089585	1.594500	7.0346
2000	1.75	25.523953	2.087941	1.594516	7.0327

Table 1. Vertical resolution benchmarking test case results. The shown firn, lake and lid depths are the numbers at the end of the 140-day simulation. Total melt is in units of metres, as the test case is in 1-D.

3 Test Cases

To test the performance and accuracy of the model numerics, we consider two test cases: the 1-D column model alone and an idealized case of melt on a surface with three Gaussian depressions.

3.1 1-D Benchmarking Study

In order to test the sensitivity of the model to the vertical resolution of the firn column, a simple 1D test case was constructed. This test was designed to force the creation of a lake, and then create a frozen lid on top of the lake. The test runs for 140 days, 60 of which are very warm (in which case the firn melts and a lake forms/grows), and 80 of which are cold (in which case the frozen lid forms). The firn column is initialised at a height of 35 m, with a surface density of 500 kg m^{-3}. Table 1 shows the results of this benchmarking case.

From Table 1 it can be seen that MONARCHS converges with respect to vertical resolution. Lake depths vary on the order of 3% when using 17.5 cm vs 1.75 cm vertical resolution, with even smaller variation in the lid and firn depths. Running with higher vertical resolution significantly increases runtime. We therefore recommend use of vertical grid spacing of 10 cm or finer, as a tradeoff between accuracy and runtime.

3.2 Gaussian Test Case

A second test case with the full 3-D model was run with an idealized topography including three depressions in the ice height, in order to demonstrate the capability of MONARCHS to transport water laterally, and test whether the inclusion of lateral flow enhanced or dampened the sensitivity to vertical resolution. For this test, a 20 x 20 grid was used, with one large Gaussian region of lower firn height in the centre, and two smaller low-height regions in the upper left and lower right domain corners (Figure 8a). The same initial forcing was used for the 1-D case shown above; an initially very high SW/LW radiation and

https://doi.org/10.5194/egusphere-2026-3247
Preprint. Discussion started: 13 July 2026

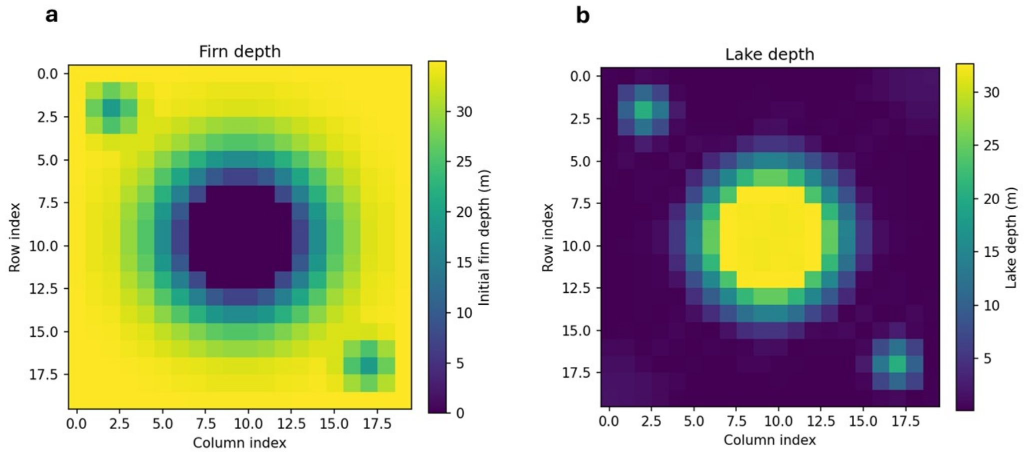

Figure 8. The Gaussian test case including two smaller topographical lows in the top left and bottom right corners with plots showing (a) initial firn height and (b) final lake depth. For this figure, 500 vertical points were used for the firn column.

temperature, followed by a cooler period. In this case however, the cooler period temperature is insufficiently cold to trigger lid formation. This allows the water to flow freely within the model domain to demonstrate the lateral flow algorithm.

In this simulation all three lakes initially fill, but as the smaller lakes become full they overflow, with additional water feeding into the large central lake. Figure 8b shows the three lake basins filled at the end of the simulation.

Experiments were run with varying vertical resolution in the firn column, similarly to the 1-D experiment above. Inclusion of lateral flow does not meaningfully change the convergence of the model results with respect to vertical resolution - mean lake depth differed by less than 4% between the runs with 17.5 cm vs 1.75 cm vertical resolution, with total melt and maximum lake depth differing by less than 2%.

4 George VI Ice Shelf Case Study

In order to demonstrate the performance of MONARCHS for a realistic ice shelf domain and forcing, we present a case study on the George VI Ice Shelf on the Antarctic Peninsula, which has experienced significant surface melt and lake formation during Austral summer in recent years (Banwell et al., 2024). MONARCHS is run over a 100 by 100 uniform horizontal grid, initialized with 500 vertical grid cells in the firn. Vertical cell depth is determined by the depth of the firn specified by the digital elevation model (DEM) used. These choices result in an approximate horizontal resolution of 1 km and average vertical resolution of approximately 10 cm. Here we use the Reference Elevation Model of Antarctica (REMA) 100 m mosaic tiles

https://doi.org/10.5194/egusphere-2026-3247
Preprint. Discussion started: 13 July 2026

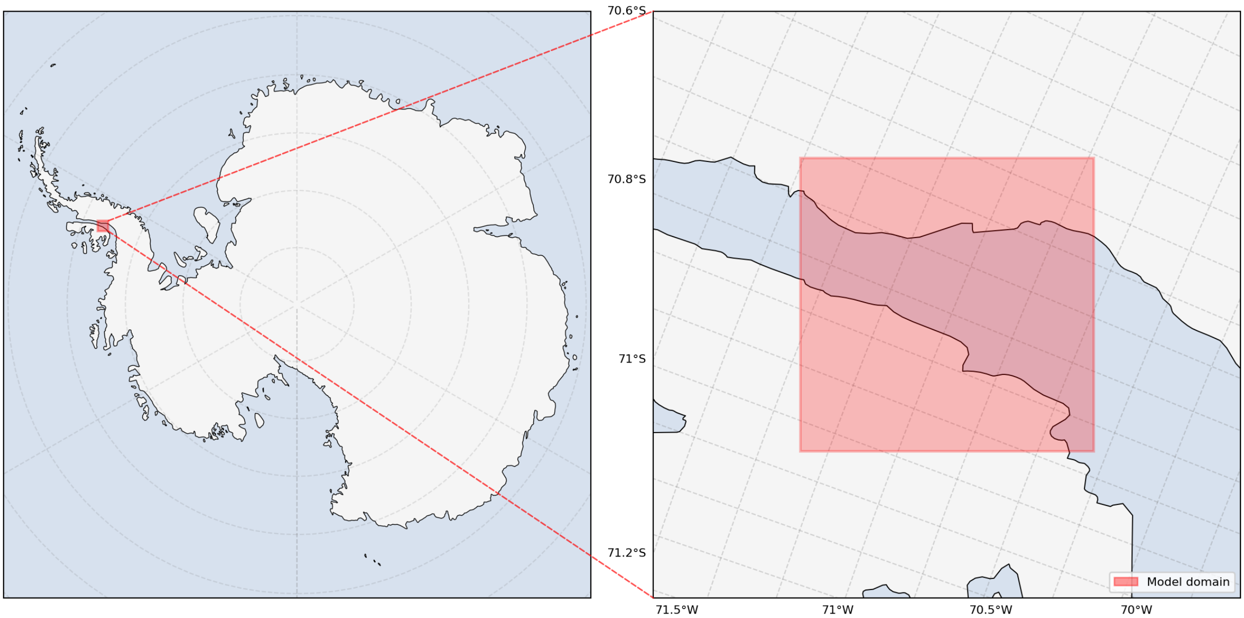

Figure 9. The George VI Ice shelf case study showing the location of ice shelf (left) and the model domain for this case study (right, red box).

(Howat et al., 2019) to provide surface elevations for this purpose. For the George VI Ice Shelf we use tile 38_12, that covers an area contained within approximately 69-70.25 °W and 71.1-71.4 °S. The precise model domain is shown in Figure 9.

MONARCHS had been designed to take input data from a variety of sources using built-in functions. Automatic weather station (AWS) data where available, reanalysis data, or climate model output all provide possible sources for the surface energy fluxes and snowfall. This case study was forced with data from the ERA-5 reanalysis product (Hersbach et al., 2020), which includes all variables necessary to calculate the surface energy balance and addition of precipitation. The model is run with a timestep of 1 hour from Jan. 1 2014 to Jan 1. 2021. Each of these simulations take approximately 6 hours running on 64 cores of a Linux processing server.

Initial temperature and density profiles are sparsely available from field measurements. However, since Buzzard et al. (2018b) found that the influences in these initial conditions were largely lost during the spin-up period here we use an empirically calculated initial density profile following Schytt (1958) as presented in Paterson (2000),

$$\rho = 917 - (917 - \rho_{sfc}) * e^{(-(1.9/z_t)*z)}. \tag{9}$$

Here ρ_{sfc}, the surface density, is initially set to 500 kgm^{-3} and z_t, the location of the firn-ice transition, is set to 37 m following Buzzard et al. (2018b). The initial temperature profile used is linear from 263.15 K at the surface to 253.15 K at the bottom of the model domain (i.e. 10 and 20 K below freezing) following Buzzard (2017).

https://doi.org/10.5194/egusphere-2026-3247
Preprint. Discussion started: 13 July 2026

As is typical for Digital Elevation Models, REMA measures height above sea-level, leading to some grid cells having zero or negative heights as the ice shelf is floating with much of its thickness below sea level. In order to ensure the firn in these grid cells can exist within the model domain we assume that the firn column is at least 20 m thick at its lowest point within all valid grid cells. To prevent this assumption from affecting the topography we add an equal amount of vertical domain to the firn column everywhere, to ensure that the relative height difference between all cells is maintained. As we are not modelling basal processes on the ice shelf or any temperature changes deep within the ice this should not affect our results.

In Figure 10 we show the output of this case study. Some of the key ERA5 surface forcing variables are shown in Figure 11. At the time of modelled maximum lake coverage, 25th January 2020, model output shows lakes forming over the ice shelf surface, with a mean lake depth at this time of 0.26 m and a maximum depth found of 3.06 m. Extensive firn densification and ice lens formation occurs as meltwater refreezes leading to loss of firn air content. Figure 10b shows the firn height changes associated with meltwater formation and movement with some areas seeing a loss of mass and others a gain where water pools in topographical lows. It can be seen from Figure 11a that the height increase in the North East (top right) of the model domain is associated with an area of high snow accumulation.

5 Validation

In order to validate our modelled surface melt lake depths we use satellite-based products of lake depth and extent. Moussavi et al. (2020a) use data from Landsat 8 imagery collated from the 2013-2020 period to map lake depths across Antarctica's ice shelves, which were derived using the methodology described in Moussavi et al. (2020b). We also use melt lake extent maps from Dirscherl et al. (2021) to evaluate MONARCHS' output. These maps have been created from Sentinel-1 (synthetic aperture radar) and Sentinel-2 (optical) data at 10 m spatial resolution and bi-weekly temporal resolution. A grid-scale comparison of the George VI case study MONARCHS output and the two observational datasets is not possible due to the different spatial scales of the products and model output. Nevertheless, comparisons of total coverage of lakes and lake depths over the model domain area are still informative.

We compared MONARCHS with the Moussavi et al. (2020a) and Dirscherl et al. (2021) Antarctic supraglacial lake datasets for 25th January 2020, the date of maximum lake coverage simulated by MONARCHS for the 2019-20 melt season, a year of high melt. For each of the validation datasets we chose the closest available time to this date. A comparison of the model output to these two observational datasets is shown in Figure 12. As lakes are only found in the Moussavi et al. (2020a) and Dirscherl et al. (2021) products in the North West of the model domain we restrict our evaluation to this area.

Even with the differences in resolution noted, large meltwater features are found in the MONARCHS output that are consistent with observations. For example, the horseshoe shaped area of lake coverage in the North West (top right) of the model domain is distinctive across Figure 12.

MONARCHS also performed well in terms of overall lake coverage, finding 22.78% lake coverage compared with Moussavi et al. (2020a)'s 16.92% and Dirscherl et al. (2021)'s 18.68% for the 2019-20 maximum as shown in Figure 13.

https://doi.org/10.5194/egusphere-2026-3247
Preprint. Discussion started: 13 July 2026

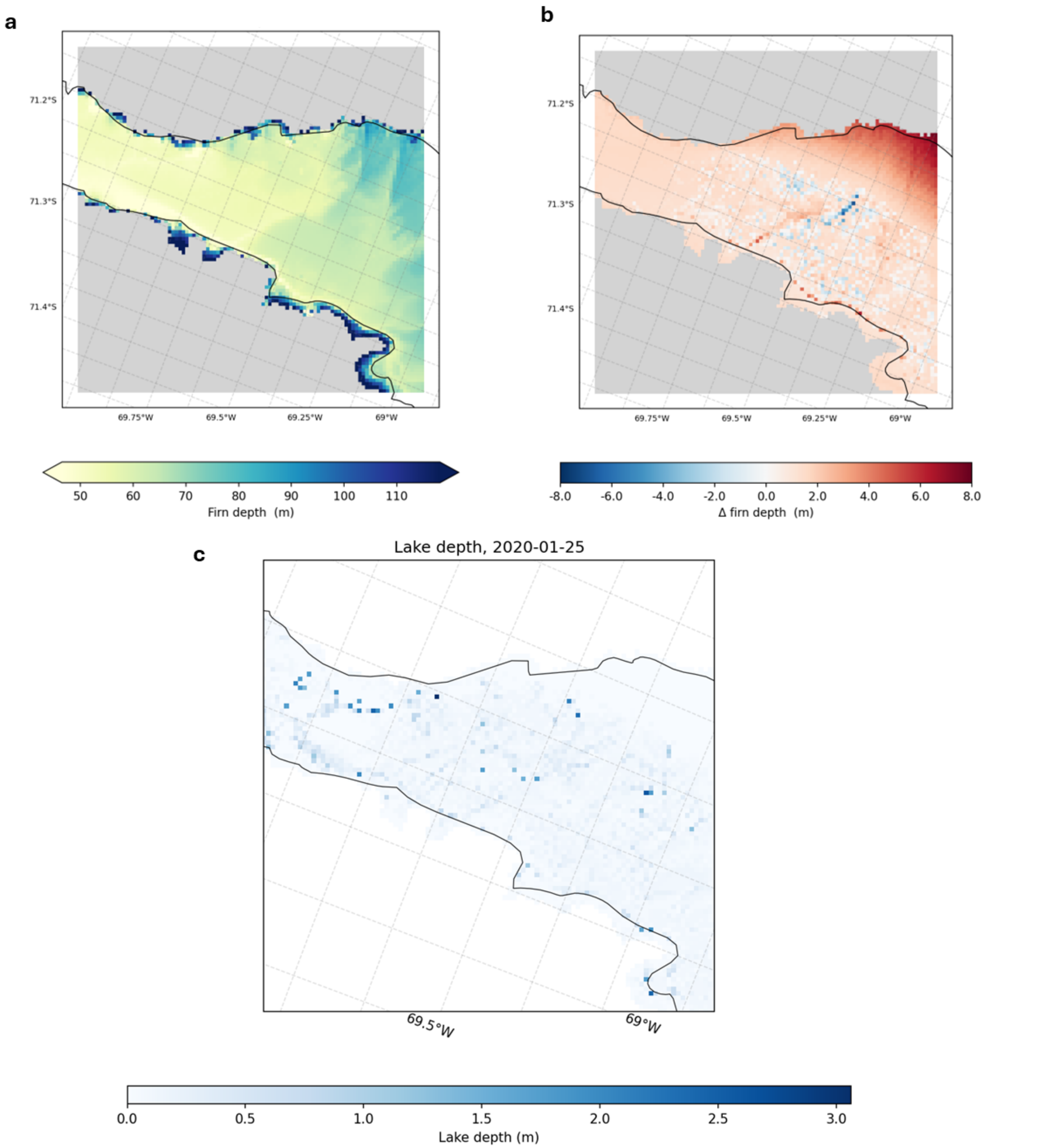

Figure 10. The George VI Ice shelf case study with (a) a map of the model domain with initial firn depths (m) shown, (b) the change in firn depth (m) from the initial conditions to the time of modelled maximum lake coverage, 25th January 2020 and (c) lake depths (m) at the time of modelled maximum coverage.

https://doi.org/10.5194/egusphere-2026-3247
Preprint. Discussion started: 13 July 2026

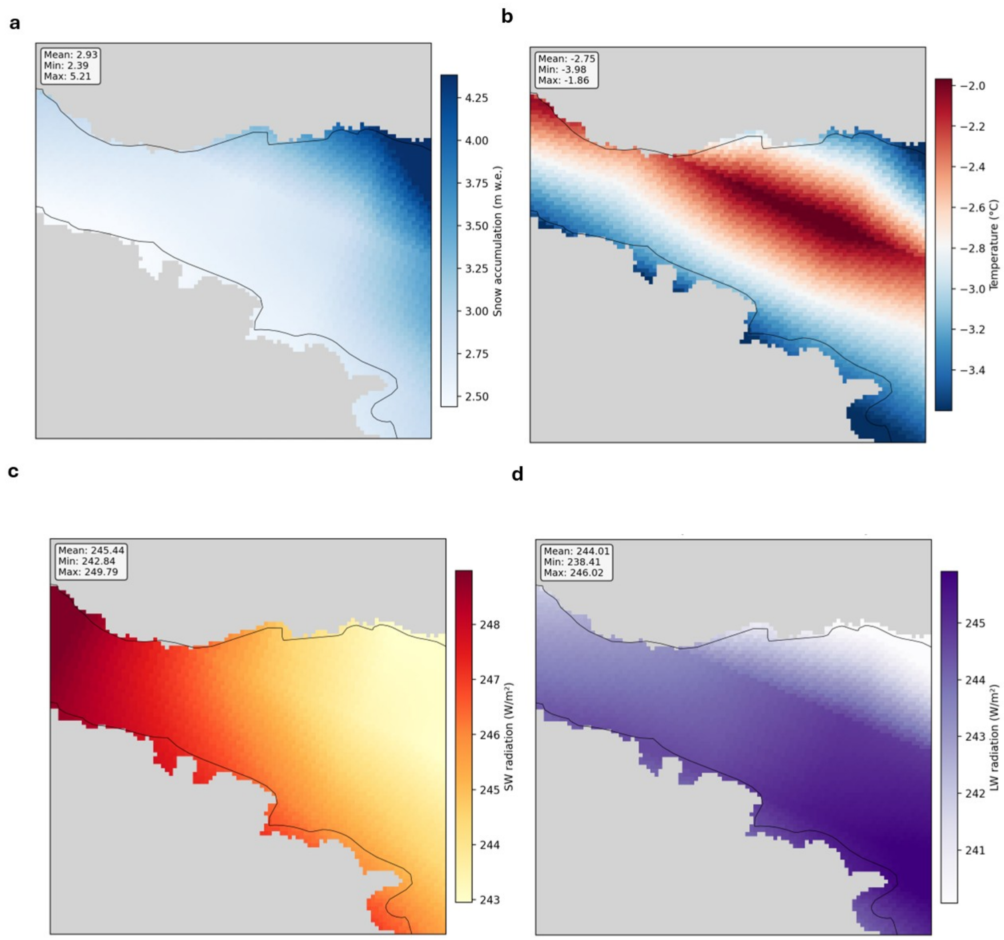

Figure 11. The ERA5 forcing used for the George VI Ice Shelf case study: (a) total snow accumulation during the model run up to the point of maximum lake coverage in 2020 shown in Figure 10 (25th January 2020) and the average surface forcing for 2019-2020 for (b) air temperature (K), (c) incoming shortwave radiation (Wm^{-2}) and (d) incoming longwave radiation (Wm^{-2}).

https://doi.org/10.5194/egusphere-2026-3247
Preprint. Discussion started: 13 July 2026

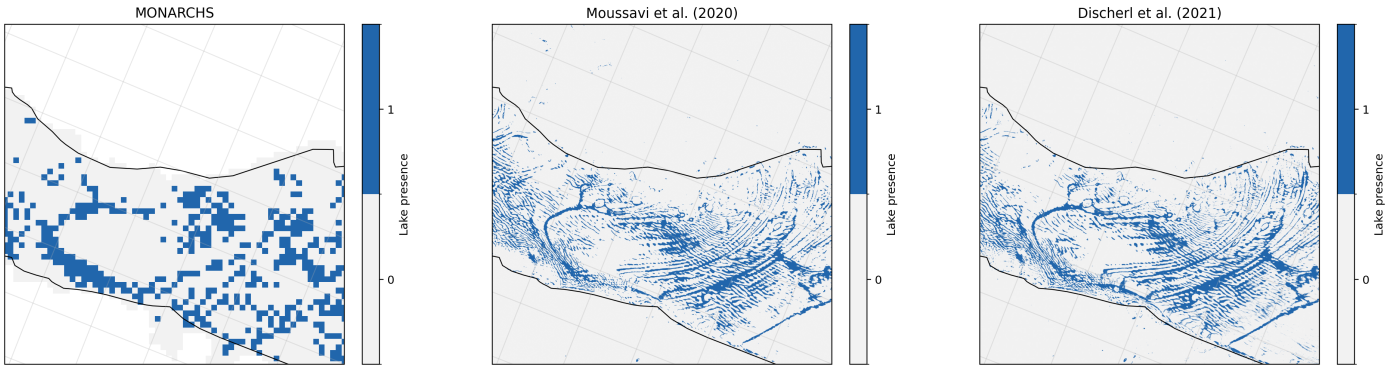

Figure 12. Lake presence over the George VI Ice shelf for high melt period, 25th January 2020, for (left) MONARCHS modelled lake output, (centre) Moussavi et al. (2020a) lakes derived from Landsat-8 from 8 scenes (18th January-1st February 2020) and (right) Dirscherl et al. (2021) lake coverage derived from Sentinel-1 and Sentinel-2 from 2 composites (18th January- 1st February 2020).

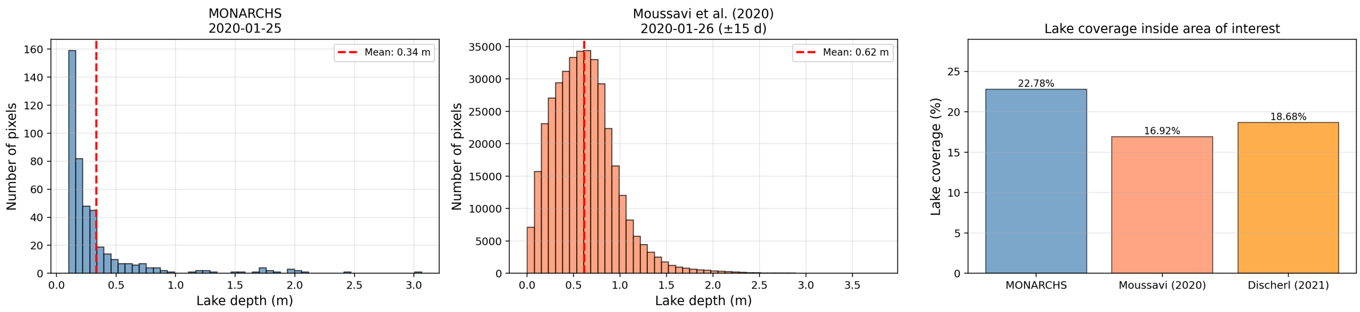

Figure 13. Lake depth over the George VI Ice shelf for 25th January 2020 for (left) MONARCHS modelled lake depth output, (centre) Moussavi et al. (2020a) lake depth derived from Landsat-8 and (right) modelled and observed lake coverage

In Figure 13 we can see that while the lakes produced by MONARCHS are of similar depths to those in Moussavi et al. (2020a), the mean lake depth in MONARCHS is 0.27 m lower than those of Moussavi et al. (2020a). For the high melt season 2019-2020, given that the lake coverage of MONARCHS was higher than that found by Moussavi et al. (2020a) this is somewhat reassuring, suggesting that overall melt amounts are similar, but the melt is more spread out horizontally in MONARCHS, which would be expected due to the lower resolution of the model compared to observations. This however is difficult to validate fully using observations as the volume of melt that is held within the firn and not contained in a lake is not accounted for by the observational products used here. Furthermore, estimates of total melt from observations from satellite altimetry still require firn models to calculate a melt volume (Otosaka et al., 2023) so it is currently impossible to validate this total melt purely by observation.

As noted previously, we would expect differences in lake coverage between the model and observations due to the spatial scales used. However, the occurrence of shallow lakes in the South East (bottom right of Figure 10c) of the model domain that

https://doi.org/10.5194/egusphere-2026-3247
Preprint. Discussion started: 13 July 2026

were not found in the observational data warrants further investigation. In Figure 11 we can see in the ERA5 data used for the surface forcing that both incoming longwave and shortwave radiation are higher in the South East of the model domain, and air temperatures are higher in the East than the West. This suggests that the South East region of the model domain would be experiencing a positive surface energy balance (and thus heating of the firn and ultimately meltwater production) at least as often, if not more so, that the rest of the model domain, so the occurrence of these lakes in the model will be as a direct result of this.

While it is possible that lakes do exist in the South East region of the domain and have not been detected in the observational datasets due to limitations of satellite coverage, cloud cover and the minimum lake depth needed for detection, there are several possibilities for why they could be occurring in the model but not forming on the actual ice shelf. Firstly, reanalysis data is known to show systematic differences and biases especially over the polar regions (Carter et al., 2022), so the lakes may be occurring due to the model forcing not representing reality.

However, without reliable firn depth and density measurements across the George VI Ice Shelf, it is possible that there is more firn air content available for meltwater retention than our initial conditions suggest, meaning that meltwater is being retained in the firn but not saturating it fully to lead to lake formation. Alternatively, as the speed of lateral movement of meltwater in the firn is a large uncertainty and also related to the unknown initial firn density profile it is possible that meltwater is either moving too far or not far enough across the ice shelf leading to lakes forming outside of their observed range. Furthermore, the modeled lakes found in this South East region are mostly shallow and therefore may be more like slush which would not be detected in the Moussavi et al. (2020a) and Dirscherl et al. (2021) products.

For a more direct comparison it is possible to coarsen the observational data to match the resolution of MONARCHS. Doing this necessitates a choice in the percentage lake coverage of an coarsened observed grid cell area used to determine if that grid cell is classified as a lake. We found that our modeled results fell within the range of lake coverage found in both observational data sets when this threshold is set to 30-40% coverage needed for a coarsened observational grid cell to be classified as a lake. With a threshold of 30% MONARCHS's coverage was within 1% of the coverage value found in Moussavi et al. (2020a) and 2.5% of the coverage found in Dirscherl et al. (2021).

While lake location is heavily influenced by the topography of the DEM used to initialize the model and the lakes in MONARCHS were found at locations of topographical lows, the volume of water able to reach these lows is highly dependent on the rate at which it is able to move through the firn. The lateral flow speed of meltwater has been noted as a large uncertainty in firn hydrology modelling (The Firn Symposium Team, 2024). Therefore we carried out sensitivity studies to determine the influence of this parameter on lake formation which are detailed in Section 5.1.

5.1 Sensitivity Study

The sensitivity of surface melt to the parameters that influence the vertical processes modelled in MONARCHS was investigated comprehensively in Buzzard et al. (2018a). There it was found that the 1-D model was most sensitive to air temperature and incoming shortwave radiation. However, through introducing lateral flow within MONARCHS, we have a further parameter to consider; the lateral flow speed. The speed of water movement within firn is a one of the key uncertainties in firn science

https://doi.org/10.5194/egusphere-2026-3247
Preprint. Discussion started: 13 July 2026

Lateral Flow speed (m/s)	Mean lake depth (m)	Max lake depth (m)	% lake coverage
No lateral flow	0.1722	1.3971	76.46
-50%	0.3044	3.3452	26.07
-10%	0.3449	3.3846	25.61
Case Study Baseline	0.2562	3.0631	25.48
+10%	0.2481	3.0835	25.59
+50%	0.2472	4.3986	25.50
+100%	0.2525	4.1881	24.62

Table 2. Outputs of sensitivity studies varying the lateral flow speed of meltwater transport for the George VI Ice Shelf case study. Here output is compared on 2020-01-25 for each run. The mean lake depth is determined as the average depth of all lakes above the lake formation threshold (0.1 m).

(The Firn Symposium Team, 2024). Therefore we investigate the impact of lateral flow speed on melt lake development. Our findings from increasing and decreasing the flow speed by 10%, 50% and 100% and removing lateral flow all together are shown in Tables 2 and 3. All results are shown for the day with maximal lake coverage in the baseline simulation for the 2018-19 and 2019-20 melt seasons presented in Section 4.

Both sets of simulations demonstrate that lateral flow of meltwater plays a key role in determining lake coverage. The influence varied depending on the melt year; including lateral flow led to increases of lake coverage of over ten times in the low melt year as melt was moved to new areas, whereas for the high melt year lake coverage decreased when lateral flow was included as melt was transported to topographical lows that were already occupied by lakes. In both high and low melt years including any lateral flow increased mean lake depths.

The influence of changing the flow speed when lateral flow is allowed is complex and non-linear. The movement of water may allow it to pool in topographical lows and allow lakes to form more quickly, leading to albedo changes that result in increased melt in those locations as well as the potential for the meltwater to contribute to flexure of the ice shelf or hydrofracture, but it also may take it to areas of high firn air content where it can refreeze within the firn.

The location of lake formation and the associated albedo changes and potential for hydrofracture matters for ice shelf stability. Figure 14 shows that changes in the lateral flow speed matter for the location and depth of individual lakes. Knowing whether or not water is reaching locations vulnerable to meltwater induced damage and how long it remains there is key to determining the influence of the meltwater on ice shelf stability (Lai et al., 2020).

In the high-melt year the mean lake depth does not vary more than 5 cm across the simulations with lateral flow, suggesting that mean depth is largely determined by topography. However, both lake coverage and the maximum lake depth increase with the inclusion of slower lateral flow, but then decrease as flow increases above the baseline speed, suggesting that as water is spreading further at greater speeds more may be reaching areas of high firn air content and not contributing to lakes. This finding, however, will be highly dependent on the ice shelf examined and the initial firn conditions specified, but it does show that the choice of lateral flow speed has consequences for lake depth and location.

https://doi.org/10.5194/egusphere-2026-3247
Preprint. Discussion started: 13 July 2026

Lateral Flow speed (m/s)	Mean lake depth (m)	Max lake depth (m)	% lake coverage
No lateral flow	0.79	0.81	0.04
-50%	1.04	2.06	0.46
-10%	0.99	2.05	0.44
Case Study Baseline	1.04	3.04	0.61
+10%	0.99	1.77	0.55
+50%	1.01	1.78	0.53
+100%	0.98	1.78	0.61

Table 3. As for Table 2, but for the 2018-19 season, where there was significantly less melt and thus fewer lakes.

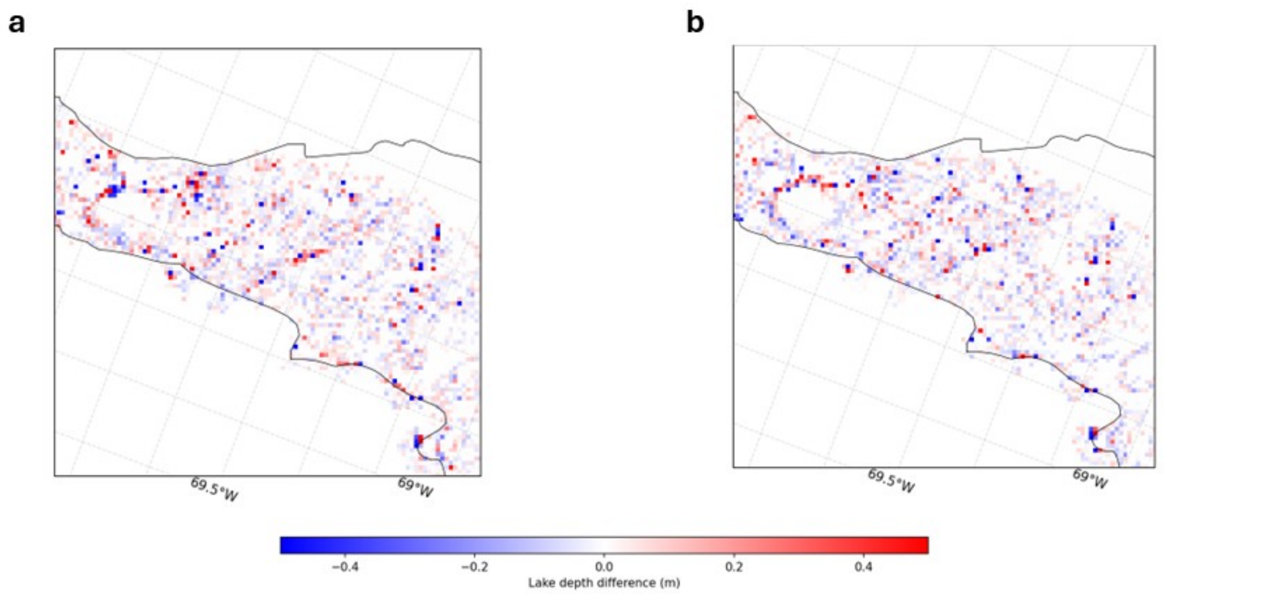

Figure 14. Lake depth difference over the George VI Ice shelf between the baseline simulation and (a) the +50% lateral flow speed simulation and (b) the -50% lateral flow speed simulation for the output shown in Table 2.

6 Discussion

Through the development of MONARCHS we have provided the community with the first open-source 3-D model of ice shelf surface hydrology and demonstrated that it is well suited to modelling meltwater transport over ice shelves and melt lake development.

The lateral flow of meltwater in firn has been identified as a key uncertainty in understanding ice mass surface hydrology (Clerx et al., 2024; Ochwat et al., 2021). Our results clearly show that lateral flow of water through firn impacts both lake coverage and depth with the sensitivity studies presented in Tables 2 and 3 demonstrating the varying impacts on lake coverage

https://doi.org/10.5194/egusphere-2026-3247
Preprint. Discussion started: 13 July 2026

and lake depth from including lateral flow. Here we examine this process within the context of a limited model domain but in reality water may be able to travel further than we simulated. While the flow speeds within firn are uncertain, the development of preferential flow pathways and surface rivers will increase this flow even further. Without understanding the speed of this lateral meltwater flow, we are systematically unable to determine how far meltwater can travel within firn and the consequences of this (Dell et al., 2020).

In the high melt year presented in the case study a large proportion of shallow lakes (10 cm) were simulated. Given MONARCHS cannot simulate lakes less than 10 cm deep due to the limitations of vertical resolution, it is likely that very shallow lakes, or slush would be present in reality in such circumstances. Slush can increased melt production through albedo change, refreeze and form impermeable ice lenses and provide water for lateral transport (Dell et al., 2024). Not accounting for slush explicitly may mean that the melt levels calculated here are underestimated and further work can be done to understand this transition stage between firn and lake.

In addition to movement of water across the ice shelf, lake and meltwater drainage are also important aspects to consider. While in MONARCHS we currently only allow water to leave the model domain at the boundaries, processes such as draining through crevasses, lake drainages (Banwell et al., 2013), waterfalls (Bell et al., 2018) and estuary formation may play an important role in evacuating water from the ice shelf surface and may go some way to explain the greater lake coverage found in MONARCHS when compared to observations in the case study presented here. Feedbacks between water flow and ice surface topography could be included in future MONARCHS development to move towards a fully dynamic model of ice shelf flexure and flow erosion at the surface.

The resolution at which MONARCHS is run is flexible depending on the research question. Although it is expensive to run simulations of higher resolution over large areas of an ice shelf such as those shown in Figure 10, a smaller subset of the model domain could be run at a higher resolution to investigate the evolution of individual lakes or small areas of lakes in more detail. This however may mean assumptions would need to be made about the amount of lateral flow entering and leaving the model domain should the domain be small enough that water influencing lake formation there will be produced elsewhere on the ice shelf.

How the distribution of firn may change in the future is key to the evolution of supraglacial meltwater systems. The predicted future loss of firn air content (Veldhuijsen et al., 2024; Dunmire et al., 2024) will reduce available pore space for meltwater retention and may lead to lakes and other supraglacial hydrological features forming more quickly, and could ultimately lead to greater firn loss and ice shelf instability. Models like MONARCHS will be key to understanding future firn air content loss and the implications for ice shelf evolution.

7 Conclusions and Future work

Here we present the first comprehensive model for Antarctic ice shelf surface hydrology, MONARCHS. We have updated the Buzzard et al. (2018a) 1-D model of ice shelf lake development and developed a new model consisting of a grid of these

https://doi.org/10.5194/egusphere-2026-3247
Preprint. Discussion started: 13 July 2026

vertical columns, allowing us to incorporate topography-dependent lateral flow of meltwater. We demonstrate the impact of this lateral flow on lake coverage and evolution through a case study on the George VI Ice Shelf.

The strong parallelization of MONARCHS permits variation of vertical and lateral resolution over wide ranges, making the model easily scalable for both larger studies of the evolution of the surface of an entire ice shelf or process-based studies (e.g. ice shelf flexure in response to meltwater loading following MacAyeal et al. (2021)). Still, higher resolution process-based studies may require a method to calculate meltwater transport at the model boundaries.

For studies of future climate and ice sheet evolution, the possibility of having areas of saturation still present in the firn column at the start of the melt season will need to be fully accounted for. Although perennial aquifers have yet to be observed directly on the Antarctic continent, it is possible that they may occur (van Wessem et al., 2021), with the possibility increasing in a warming climate. While MONARCHS can allow water to remain in the firn, the evolution of firn aquifers or buried lakes is a complex process that requires further understanding.

Furthermore, ongoing work into the permeability of ice lenses and ice slabs (e.g. Laha and Mair (2025)) could be incorporated into the model to allow slow percolation of water through the ice lens as oppose to assuming it all either stays above the lens or runs off. The importance of this process in an Antarctic setting is yet to be determined, but sensitivity testing of ice slab permeability using MONARCHS could be used to investigate this.

MONARCHS is created to be a community model and thus we welcome suggestions for its development for additional uses.

8 Code and data availability

The documentation/ user manual for MONARCHS is available along with model code under the GPL v3.0-or-later License at https://monarchs-ice.github.io/monarchs/index.html.

The model code used in this study is archived in a Zenodo repository at https://doi.org/10.5281/zenodo.20545354 (Elsey and Buzzard, 2026), along with the outputs for the case study described above.

https://doi.org/10.5194/egusphere-2026-3247
Preprint. Discussion started: 13 July 2026

Appendix A: MONARCHS Variables

Parameter Description	Notation	Model parameter	Units	Example Value
Air pressure	p	p	Pa	Determined by surface forcing data
Air temperature (10 m)	T_{air}	T_{air}	K	Determined by surface forcing data
Albedo	α	alpha	dimensionless	0.8670/ 0.6 (dry/wet snow albedo)
				0.413 (exposed water albedo)
				lake albedo varies with lake depth
Density of firn	ρ	calculated from Sfrac/ Lfrac	kgm^{-3}	variable
Density of ice	ρ_{ice}	rho_ice	kgm^{-3}	917
Density of water	ρ_{liq}	rho_liq	kgm^{-3}	1000
Flow speed	u	u	ms^{-2}	calculated within model
Hydraulic permeability	Π	Big_pi	m^{2}	-2.53 x 10^{-10}
Incoming longwave energy	F_{LW}	LW_in	Wm^{2}	Determined by surface forcing data
Incoming shortwave energy	F_{SW}	SW_in	Wm^{2}	Determined by surface forcing data
Latent heat flux	F_{lat}	F_lat	W m^{2}	Determined by surface forcing data
Acceleration due to gravity	g	g	m s $^{-2}$	9.8
Latent heat of fusion (water)	$\mathcal{L}$	L	Jkg^{-1}	334000
Liquid fraction	n/a	Lfrac	dimensionless	Varies between 0-1
Pore closure density	ρ_{pc}	pore_closure	kgm^{-3}	830
Sensible heat flux	F_{sens}	F_sens	Wm^{2}	Determined by surface forcing data
Solid fraction	ϕ	Sfrac	dimensionless	Varies between 0-1
Specific heat capacity (air)	$c_{p_{air}}$	cp_air	Jkg$^{-1}K^{-1}$	1004
Specific heat capacity (water)	$c_{p_{liq}}$	cp_water	Jkg$^{-1}K^{-1}$	4217
Stefan-Boltzman constant	σ	sigma	Wm^{-2} K^{-4}	5.67 x 10^{-8}
Surface emissivity	ϵ	epsilon	dimensionless	Ranges from 0 to 1
Thermal diffusivity (air)	κ_{air}	k_{air}	m$^{2}s^{-1}$	0.022
Thermal diffusivity (water)	κ_{liq}	k_water	m$^{2}s^{-1}$	0.5818
Viscosity	η	eta	Pas^{-1}	1.787 x 10^{-3}
Wind speed	w	w	ms^{-2}	determined by surface forcing data

Table A1. The standard parameters used in MONARCHS with the parameter description, notation used in this paper, parameter name in the MONARCHS code, units and example value used in the case study presented here.

https://doi.org/10.5194/egusphere-2026-3247
Preprint. Discussion started: 13 July 2026

Author contributions. SB and AR conceptualized this study. SB and JE carried out coding and implementation of case studies. All authors contributed to model design and development and manuscript preparation. This project was funded by NASA Award 80NSSC20K1131.

Competing interests. No competing interests are present.

Acknowledgements.

https://doi.org/10.5194/egusphere-2026-3247
Preprint. Discussion started: 13 July 2026

References

Banwell, A. F. and MacAyeal, D. R.: Ice-shelf fracture due to viscoelastic flexure stress induced by fill/drain cycles of supraglacial lakes, Antarctic Science, 27, 587–597, https://doi.org/10.1017/S0954102015000292, 2015.

Banwell, A. F., Arnold, N. S., Willis, I. C., Tedesco, M., and Ahlstrm, A. P.: Modeling supraglacial water routing and lake filling on the Greenland Ice Sheet, Journal of Geophysical Research F: Earth Surface, 117, 1–11, https://doi.org/10.1029/2012JF002393, 2012.

Banwell, A. F., MacAyeal, D. R., and Sergienko, O. V.: Breakup of the Larsen B Ice Shelf triggered by chain reaction drainage of supraglacial lakes, Geophysical Research Letters, 40, 5872–5876, https://doi.org/10.1002/2013GL057694, 2013.

Banwell, A. F., Willis, I. C., Stevens, L. A., Dell, R. L., and MacAyeal, D. R.: Observed meltwater-induced flexure and fracture at a doline on George VI Ice Shelf, Antarctica, Journal of Glaciology, 70, e47, https://doi.org/10.1017/jog.2024.31, https://www.cambridge.org/core/product/identifier/S0022143024000315/type/journal_article, 2024.

Bell, R. E., Chu, W., Kingslake, J., Das, I., Tedesco, M., Tinto, K. J., Zappa, C. J., Frezzotti, M., Boghosian, A., and Lee, W. S.: Antarctic ice shelf potentially stabilized by export of meltwater in surface river, Nature, 544, 344–348, https://doi.org/10.1038/nature22048, http://dx.doi.org/10.1038/nature22048, 2017.

Bell, R. E., Banwell, A. F., Trusel, L. D., and Kingslake, J.: Antarctic surface hydrology and impacts on ice-sheet mass balance, Nature Climate Change, 8, 1044–1052, https://doi.org/10.1038/s41558-018-0326-3, http://dx.doi.org/10.1038/s41558-018-0326-3, 2018.

Boxall, K., Christie, F. D. W., Willis, I. C., Wuite, J., and Nagler, T.: Seasonal land-ice-flow variability in the Antarctic Peninsula, The Cryosphere, 16, 3907–3932, https://doi.org/10.5194/tc-16-3907-2022, https://tc.copernicus.org/articles/16/3907/2022/, 2022.

Buzzard, S.: A Mathematical Model of Melt Lake Formation on an Ice Shelf., https://doi.org/https://doi.org/10.17864/1947.121, 2017.

Buzzard, S., Feltham, D., and Flocco, D.: Modelling the fate of surface melt on the Larsen C Ice Shelf, Cryosphere, 12, https://doi.org/10.5194/tc-12-3565-2018, 2018a.

Buzzard, S., Feltham, D., and Flocco, D.: A Mathematical Model of Melt Lake Development on an Ice Shelf, Journal of Advances in Modeling Earth Systems, 10, https://doi.org/10.1002/2017MS001155, 2018b.

Carter, J., Leeson, A., Orr, A., Kittel, C., and van Wessem, J. M.: Variability in Antarctic surface climatology across regional climate models and reanalysis datasets, The Cryosphere, 16, 3815–3841, https://doi.org/10.5194/tc-16-3815-2022, https://tc.copernicus.org/articles/16/3815/2022/, 2022.

Chase, C. G.: Fluvial landsculpting and the fractal dimension of topography, Geomorphology, 5, 39–57, https://doi.org/10.1016/0169-555X(92)90057-R, 1992.

Clerx, N., Machguth, H., Tedstone, A., and van As, D.: Modelling lateral meltwater flow and superimposed ice formation atop Greenland's near-surface ice slabs, Journal of Glaciology, 70, e54, https://doi.org/10.1017/jog.2024.69, 2024.

Colbeck, S. C.: The physical aspects of water flow through snow, vol. 11, Academic, San Diego, Calif,, 1978.

Cooper, M. G., Smith, L. C., Rennermalm, A. K., Tedesco, M., Muthyala, R., Leidman, S. Z., Moustafa, S. E., and Fayne, J. V.: Spectral attenuation coefficients from measurements of light transmission in bare ice on the Greenland Ice Sheet, The Cryosphere, 15, 1931–1953, https://doi.org/10.5194/tc-15-1931-2021, https://tc.copernicus.org/articles/15/1931/2021/, 2021.

Coulthard, T. J., Macklin, M. G., and Kirkby, M. J.: A cellular model of Holocene upland river basin and alluvial fan evolution, Earth Surface Processes and Landforms, 27, 269–288, https://doi.org/10.1002/esp.318, 2002.

DeConto, R. M. and Pollard, D.: Contribution of Antarctica to past and future sea-level rise, Nature, 531, 591–597, https://doi.org/10.1038/nature17145, http://dx.doi.org/10.1038/nature17145, 2016.

https://doi.org/10.5194/egusphere-2026-3247
Preprint. Discussion started: 13 July 2026

Dell, R., Arnold, N., Willis, I., Banwell, A., Williamson, A., Pritchard, H., and Orr, A.: Lateral meltwater transfer across an Antarctic ice shelf, The Cryosphere, 14, 2313–2330, https://doi.org/10.5194/tc-14-2313-2020, https://tc.copernicus.org/articles/14/2313/2020/, 2020.

Dell, R. L., Willis, I. C., Arnold, N. S., Banwell, A. F., and de Roda Husman, S.: Substantial contribution of slush to meltwater area across Antarctic ice shelves, Nature Geoscience, 17, 624–630, https://doi.org/10.1038/s41561-024-01466-6, https://doi.org/10.1038/s41561-024-01466-6, 2024.

Dirscherl, M. C., Dietz, A. J., and Kuenzer, C.: Seasonal evolution of Antarctic supraglacial lakes in 2015–2021 and links to environmental controls, The Cryosphere, 15, 5205–5226, https://doi.org/10.5194/tc-15-5205-2021, https://tc.copernicus.org/articles/15/5205/2021/, 2021.

Dunmire, D., Lenaerts, J., Banwell, A., Wever, N., Shragge, J., Lhermitte, S., Drews, R., Pattyn, F., Hansen, J., Willis, I., et al.: Observations of buried lake drainage on the Antarctic Ice Sheet, Geophysical research letters, 47, e2020GL087 970, 2020.

Dunmire, D., Wever, N., Banwell, A., and Lenaerts, J.: Antarctic-wide ice-shelf firn emulation reveals robust future firn air depletion signal for the Antarctic Peninsula, Communications Earth & Environment, 5, 100, https://doi.org/10.1038/s43247-024-01255-4, https://doi.org/10.1038/s43247-024-01255-4, 2024.

Edwards, T. L., Brandon, M. A., Durand, G., Edwards, N. R., Golledge, N. R., Holden, P. B., Nias, I. J., Payne, A. J., Ritz, C., and Wernecke, A.: Revisiting Antarctic ice loss due to marine ice-cliff instability, Nature, 566, 58–64, https://doi.org/10.1038/s41586-019-0901-4, http://dx.doi.org/10.1038/s41586-019-0901-4, 2019.

Elsey, J. and Buzzard, S.: monarchs-ice/monarchs: v1.0.3, https://doi.org/10.5281/zenodo.20545354, https://doi.org/10.5281/zenodo.20545354, 2026.

Fricker, H. A., Galton-Fenzi, B. K., Walker, C. C., Freer, B. I. D., Padman, L., and DeConto, R.: Antarctica in 2025: Drivers of deep uncertainty in projected ice loss, Science, 387, 601–609, https://doi.org/10.1126/science.adt9619, https://www.science.org/doi/abs/10.1126/science.adt9619, 2025.

Gantayat, P., Banwell, A., Leeson, A., Lea, J., Petersen, D., Gourmelen, N., and Fettweis, X.: A new model for supraglacial hydrology evolution and drainage for the Greenland Ice Sheet (SHED v1.0), Geoscientific Model Development, 16, 5803–5823, https://doi.org/10.5194/gmd-16-5803-2023, 2023.

Grau, D., Hussain, A., and Robel, A. A.: Predicting mean depth and area fraction of Antarctic supraglacial melt lakes with physics-based parameterizations, Nature Communications, 16, 6518, 2025.

Hanna, E., Topál, D., and Box, J. e. a.: Short- and long-term variability of the Antarctic and Greenland ice sheets, Nat Rev Earth Enviro, 5, 193—-210, 2024.

Hersbach, H., Bell, B., Berrisford, P., Hirahara, S., Horányi, A., Muñoz-Sabater, J., Nicolas, J., Peubey, C., Radu, R., Schepers, D., Simmons, A., Soci, C., Abdalla, S., Abellan, X., Balsamo, G., Bechtold, P., Biavati, G., Bidlot, J., Bonavita, M., Chiara, G. D., Dahlgren, P., Dee, D., Diamantakis, M., Dragani, R., Flemming, J., Forbes, R., Fuentes, M., Geer, A., Haimberger, L., Healy, S., Hogan, R. J., Hólm, E., Janisková, M., Keeley, S., Laloyaux, P., Lopez, P., Lupu, C., Radnoti, G., Rosnay, P. d., Rozum, I., Vamborg, F., Villaume, S., and Thépaut, J.-N.: The ERA5 global reanalysis, Quarterly Journal of the Royal Meteorological Society, 146, 1999–2049, https://rmets.onlinelibrary.wiley.com/journal/1477870x, publisher: John Wiley & Sons, Ltd, 2020.

Hock, R.: Glacier melt: a review of processes and their modelling, Progress in Physical Geography: Earth and Environment, 29, 362–391, https://doi.org/10.1191/0309133305pp453ra, https://doi.org/10.1191/0309133305pp453ra, 2005.

Holland, P. R., Brisbourne, A., Corr, H. F. J., Mcgrath, D., Purdon, K., Paden, J., Fricker, H. A., and Paolo, F. S.: Oceanic and atmospheric forcing of Larsen C Ice-Shelf thinning, pp. 1005–1024, https://doi.org/10.5194/tc-9-1005-2015, 2015.

Howat, I. M., Porter, C., Smith, B. E., Noh, M.-J., and Morin, P.: The Reference Elevation Model of Antarctica, The Cryosphere, 13, 665–674, https://doi.org/10.5194/tc-13-665-2019, https://tc.copernicus.org/articles/13/665/2019/, 2019.

Kingslake, J., Ely, J. C., Das, I., and Bell, R. E.: Widespread movement of meltwater onto and across Antarctic ice shelves, Nature, 544, 349–352, https://doi.org/10.1038/nature22049, http://dx.doi.org/10.1038/nature22049, 2017.

Kingslake, J., Trusel, L. D., Banwell, A. F., Bell, R. E., Das, I., Deconto, R. M., Tedesco, M., Lenaerts, J. T. M., and Schoof, C.: Antarctic Surface Hydrology & Ice-Shelf Stability Workshop Report, 2019.

Kou, L., Labrie, D., and Chylek, P.: Refractive indices of water and ice in the 0.65-to 2.5-μm spectral range, Applied optics, 32, 3531–3540, 1993.

Kuipers Munneke, P., Luckman, A. J., Bevan, S. L., Smeets, C. J. P. P., Gilbert, E., van den Broeke, M. R., Wang, W., Zender, C., Hubbard, B., Ashmore, D., Orr, A., King, J. C., and Kulessa, B.: Intense Winter Surface Melt on an Antarctic Ice Shelf, Geophysical Research Letters, 45, 7615–7623, https://doi.org/https://doi.org/10.1029/2018GL077899, https://agupubs.onlinelibrary.wiley.com/doi/abs/10.1029/2018GL077899, 2018.

Laha, S. and Mair, D.: Modelling evolution of Greenland Ice Sheet near-surface ice slab and its impact on runoff, European Geosciences Union General Assembly 2025 (EGU25), held 27 April-2 May, 2025 in Vienna, Austria. Online at https://www.egu25.eu/, id. EGU25-1342, https://doi.org/10.5194/egusphere-egu25-1342, 2025.

Lai, C.-Y., Kingslake, J., Wearing, M. G., Chen, P.-H. C., Gentine, P., Li, H., Spergel, J. J., and van Wessem, J. M.: Vulnerability of Antarctica's ice shelves to meltwater-driven fracture, Nature, 584, 574–578, 2020.

Lam, S. K., Pitrou, A., and Seibert, S.: Numba: A llvm-based python jit compiler, in: Proceedings of the Second Workshop on the LLVM Compiler Infrastructure in HPC, pp. 1–6, 2015.

Leeson, A. A., Shepherd, A., Palmer, S., Sundal, A., and Fettweis, X.: The Cryosphere Simulating the growth of supraglacial lakes at the western margin of the Greenland ice sheet, pp. 1077–1086, https://doi.org/10.5194/tc-6-1077-2012, 2012.

Leppäranta, M.: Freezing of lakes and the evolution of their ice cover, Springer, 2015.

MacAyeal, D. R., Sergienko, O. V., Banwell, A. F., Macdonald, G. J., Willis, I. C., and Stevens, L. A.: Treatment of ice-shelf evolution combining flow and flexure, Journal of Glaciology, 67, 885–902, https://doi.org/10.1017/jog.2021.39, 2021.

Moussavi, M., Abdalati, W., Halberstadt, A., P. A., and Trusel, L.: Supraglacial Lakes in Antarctica, U.S. Antarctic Program (USAP) Data Center, https://doi.org/10.15784/601401, 2020a.

Moussavi, M., Pope, A., Halberstadt, A., Trusel, L., Cioffi, L., and Abdalati, W.: Antarctic Supraglacial Lake Detection Using Landsat 8 and Sentinel-2 Imagery: Towards Continental Generation of Lake Volumes., Remote Sens., 12, https://doi.org/10.15784/601401, 2020b.

Ochwat, N. E., Marshall, S. J., Moorman, B. J., Criscitiello, A. S., and Copland, L.: Evolution of the firn pack of Kaskawulsh Glacier, Yukon: meltwater effects, densification, and the development of a perennial firn aquifer, The Cryosphere, 15, 2021–2040, https://doi.org/10.5194/tc-15-2021-2021, https://tc.copernicus.org/articles/15/2021/2021/, 2021.

Otosaka, I. N., Shepherd, A., Ivins, E. R., Schlegel, N.-J., Amory, C., van den Broeke, M. R., Horwath, M., Joughin, I., King, M. D., Krinner, G., Nowicki, S., Payne, A. J., Rignot, E., Scambos, T., Simon, K. M., Smith, B. E., Sørensen, L. S., Velicogna, I., Whitehouse, P. L., A, G., Agosta, C., Ahlstrøm, A. P., Blazquez, A., Colgan, W., Engdahl, M. E., Fettweis, X., Forsberg, R., Gallée, H., Gardner, A., Gilbert, L., Gourmelen, N., Groh, A., Gunter, B. C., Harig, C., Helm, V., Khan, S. A., Kittel, C., Konrad, H., Langen, P. L., Lecavalier, B. S., Liang, C.-C., Loomis, B. D., McMillan, M., Melini, D., Mernild, S. H., Mottram, R., Mouginot, J., Nilsson, J., Noël, B., Pattle, M. E., Peltier, W. R., Pie, N., Roca, M., Sasgen, I., Save, H. V., Seo, K.-W., Scheuchl, B., Schrama, E. J. O., Schröder, L., Simonsen, S. B., Slater, T., Spada, G., Sutterley, T. C., Vishwakarma, B. D., van Wessem, J. M., Wiese, D., van der Wal, W., and Wouters, B.: Mass balance of the

Greenland and Antarctic ice sheets from 1992 to 2020, Earth System Science Data, 15, 1597–1616, https://doi.org/10.5194/essd-15-1597-2023, https://essd.copernicus.org/articles/15/1597/2023/, 2023.

Paterson, W.: The Physics of Glaciers, Butterworth-Heinemann, 2000.

Pope, A., Scambos, T. A., Moussavi, M., Tedesco, M., Willis, M., Shean, D., and Grigsby, S.: Estimating supraglacial lake depth in West Greenland using Landsat 8 and comparison with other multispectral methods, The Cryosphere, 10, 15–27, https://doi.org/10.5194/tc-10-15-2016, https://tc.copernicus.org/articles/10/15/2016/, 2016.

Pope, R. M. and Fry, E. S.: Absorption spectrum (380–700 nm) of pure water. II. Integrating cavity measurements, Applied optics, 36, 8710–8723, 1997.

Rignot, E., Jacobs, S., Mouginot, J., and Scheuchl, B.: Ice-shelf melting around antarctica, Science, 341, 266–270, https://doi.org/10.1126/science.1235798, 2013.

Scambos, T. A., Hulbe, C., Fahnestock, M., and Bohlander, J.: The link between climate warming and break-up of ice shelves in the Antarctic Peninsula, Journal of Glaciology, 46, 516–530, https://doi.org/10.3189/172756500781833043, 2000.

Scambos, T. A., Bohlander, J. A., Shuman, C. A., and Skvarca, P.: Glacier acceleration and thinning after ice shelf collapse in the Larsen B embayment, Antarctica, Geophysical Research Letters, 31, 2001–2004, https://doi.org/10.1029/2004GL020670, 2004.

Schytt, V.: Snow Studies at Maudheim: Snow Studies Inland. The Inner Structure of the Ice Shelf at Maudheim as Shown by Core Drilling, Norsk Polarinstitutt, 1958.

The Firn Symposium Team: Firn on Ice Sheets, Nat Rev Earth Enviro, 5, 79—-99, 2024.

Trusel, L. D., Frey, K. E., Das, S. B., Karnauskas, K. B., Kuipers Munneke, P., Van Meijgaard, E., and Van Den Broeke, M. R.: Divergent trajectories of Antarctic surface melt under two twenty-first-century climate scenarios, Nature Geoscience, 8, 927–932, https://doi.org/10.1038/ngeo2563, 2015.

Tuckett, P., Ely, J., and Sole, A. e. a.: Rapid accelerations of Antarctic Peninsula outlet glaciers driven by surface melt, Nat Commun, 10, https://doi.org/10.1038/s41467-019-12039-2, 2019.

Van Rossum, G. and Drake, F. L.: Python 3 Reference Manual, CreateSpace, Scotts Valley, CA, 2009.

van Wessem, J. M., Steger, C. R., Wever, N., and van den Broeke, M. R.: An exploratory modelling study of perennial firn aquifers in the Antarctic Peninsula for the period 1979–2016, The Cryosphere, 15, 695–714, https://doi.org/10.5194/tc-15-695-2021, 2021.

Veldhuijsen, S. B. M., van de Berg, W. J., Kuipers Munneke, P., and van den Broeke, M. R.: Firn air content changes on Antarctic ice shelves under three future warming scenarios, The Cryosphere, 18, 1983–1999, https://doi.org/10.5194/tc-18-1983-2024, https://tc.copernicus.org/articles/18/1983/2024/, 2024.

Wuite, J., Rott, H., Hetzenecker, M., Floricioiu, D., De Rydt, J., Gudmundsson, G. H., Nagler, T., and Kern, M.: Evolution of surface velocities and ice discharge of Larsen B outlet glaciers from 1995 to 2013, The Cryosphere, 9, 957–969, https://doi.org/10.5194/tc-9-957-2015, https://tc.copernicus.org/articles/9/957/2015/, 2015.